Response Letter to the First Reviewer

Thank you very much for the comments provided by the reviewer for this paper. We have made modifications and responses to each comment, the specific details are as follows:

Q1:

Describe clearly novelty of the paper

Responses:

Thank you very much for your questions on the performance of the proposed method. The main breakthrough of the proposed hybrid modulation method is to reduce the common-mode voltage (CMV) peak value to the minimum value in the full modulation region, also improve dynamic performance, and try to maintain steady-state performance as much as possible. It has been verified in the simulation and experiment part.

The proposed modulation method has two innovative aspects. First, we divide the whole region into LVMR, HVMR, and OVMR. In HVMR, we use NSPWM, a three voltage-vectors synthesized scheme, to best maintain the small current THD. However, NSPWM cannot eliminate the CMV in LVMR, so we use AZSPWM to cover LVMR. Second, it is about the improved overvoltage modulation PWM (IOMPWM) method. When the reference voltage exceeds the maximum modulation boundary region, especially in the start-up process, IOMPWM has the minimum error with the reference voltage vector. Therefore, IOMPWM can improve the dynamic performance.

Q2:

Because you focus on modulation the modulation gains or the accuracy of your overmodulation strategy (OVRM) should be discussed and proven in the paper

Responses:

Thank you for your suggestion: It is necessary to discuss the modulation gains of the several modulation strategies discussed before introducing the proposed method. Therefore, in the lines 139-155, the modulation gains are discussed in detail.

In Figure 3, the per-fundamental-cycle linearity regions (dark blue circular zones) and the per-PWM-cycle linearity regions (dark + light blue zones) of several modulations are illustrated. The standard SVPWM provides per-fundamental-cycle voltage linearity for $0 \le M \le 1$. The per-carrier-cycle linearity range of these modulators covers the 3-phase inverter voltage hexagon shown in Figure 3 (a). The AZSPWM methods have the same voltage linearity characteristics as SVPWM. However, RSPWM methods exhibit different characteristics. Both RSPWM1 and RSPWM2 [Figure 3 (c)] are linear inside either triangle T1 or T2, depending on which vector groups are selected. For the VVs u_1, u_3, u_5, define T_1 and VVs u_2, u_4, u_6 , define T_2. The per-fundamental-cycle linearity range of either method is $0 \le M \le 0.57$. RSPWM3 is linear inside the union of T_1 and T_2, which corresponds to a six-edged star [Figure 3 (d)]. The per-fundamental-cycle linearity of RSPWM3 is valid for $0 \le M \le 0.67$ (corresponding to the largest circle inside the star). In contrast to RSPWM methods, NSPWM is linear at high M [$0.57 \le M \le 1$, Figure 3 (b)]. In fact, these methods for some regions complement each other.

The modulation index M, is the ratio between the magnitude of $\boldsymbol{u}_{ref}$ and half of the height of the whole region hexagon and is defined as

$$M = \frac{U_{ref}}{U_{dc} / \sqrt{3}}$$

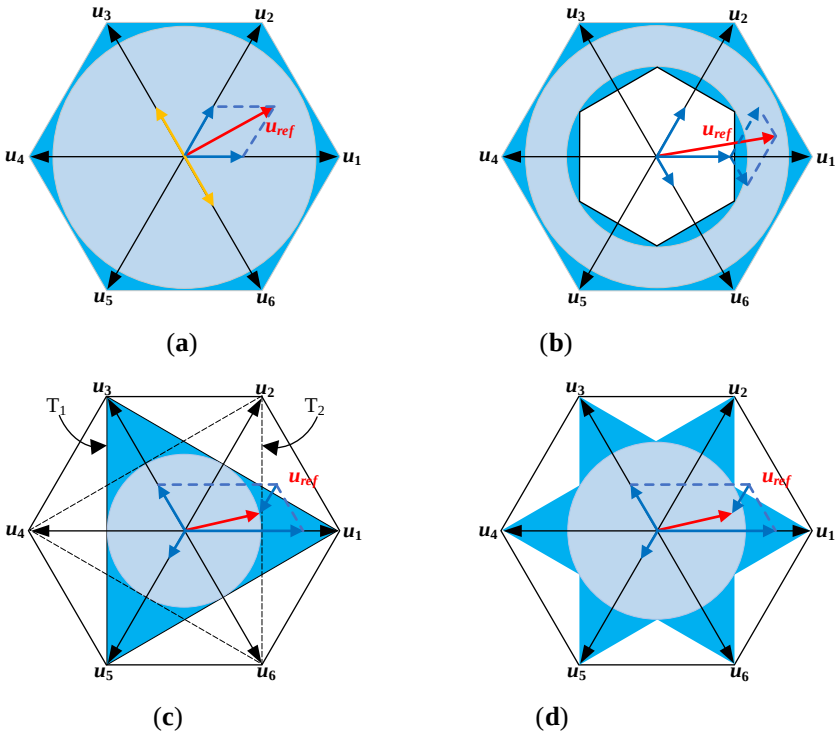

Figure 3. Voltage linearity regions. (a) SVPWM, AZSPWM. (b) NSPWM. (c) RSPWM1–2. (d) RSPWM3.

Thank you for your suggestion on the accuracy of the IOMPWM and conventional method. Below is the detail accuracy comparison calculation process.

The magnitude of u_{ref} , in Figure 8, OM is represented as:

$$\left|u_{ref}\right| = \mathrm{OM} = \sqrt{(u_\alpha^*)^2 + (u_\beta^*)^2} \tag{1}$$

In this paper, the accuracy ratio of the conventional overvoltage modulation method is defined as η_{SVPWM}, and can be derived as:

$$\eta_{SVPWM} = \frac{|\mathrm{HM}|}{|\mathrm{OM}|} \tag{2}$$

Similarly, the accuracy ratio of the proposed IOMPWM method is defined as η_{IOMPWM}, and can be derived as:

$$\eta_{IOMPWM} = \frac{|\mathrm{GM}|}{|\mathrm{OM}|} \tag{3}$$

According to the geographical relation, |HM| is larger than |GM|. Therefore η_{IOMPWM} is less than η_{SVPWM}, so compared with the conventional overvoltage modulation method, IOMPWM can obtain less error with the reference VV and generate higher i_q.

The accuracy ratio of conventional overvoltage modulation method and IOMPWM in all zones are derived in revised manuscript, and summarized in Table 5.

Table 5. Modulation accuracy for u_{ref} in all zones of OVMR.

Sector	Zone	IOMPWM	Conventional Method
I	C_{11}	$\sqrt{\frac{\frac{U_{dc}^2}{3}+(\frac{u_\alpha^*}{2}-\frac{\sqrt{3}u_\beta^*}{2})^2}{(u_\alpha^*)^2+(u_\beta^*)^2}}$	$\frac{U_{dc}}{\sqrt{3(u_\alpha^*)^2+3(u_\beta^*)^2}*\cos(\arctan(\frac{u_\beta^*}{u_\alpha^*}))}$
	C_{12}	$\sqrt{\frac{4U_{dc}^2}{9((u_\alpha^*)^2+(u_\beta^*)^2)}}$	
	C_{13}		
II	C_{21}	$\sqrt{\frac{(u_\alpha^*)^2+\frac{U_{dc}^2}{3}}{(u_\alpha^*)^2+(u_\beta^*)^2}}$	$\begin{cases}\frac{U_{dc}}{\sqrt{3(u_\alpha^*)^2+3(u_\beta^*)^2}*\cos(\arctan(\frac{u_\beta^*}{u_\alpha^*}))} & u_\alpha^*\neq 0\\ \frac{U_{dc}}{\sqrt{3(u_\alpha^*)^2+3(u_\beta^*)^2}} & u_\alpha^*=0\end{cases}$
	C_{22}	$\sqrt{\frac{4U_{dc}^2}{9((u_\alpha^*)^2+(u_\beta^*)^2)}}$	
	C_{23}		
III	C_{31}	$\sqrt{\frac{\frac{U_{dc}^2}{3}+(\frac{u_\alpha^*}{2}+\frac{\sqrt{3}u_\beta^*}{2})^2}{(u_\alpha^*)^2+(u_\beta^*)^2}}$	$\frac{U_{dc}}{\sqrt{3(u_\alpha^*)^2+3(u_\beta^*)^2}*\cos(\arctan(\frac{u_\beta^*}{u_\alpha^*}))}$
	C_{32}	$\sqrt{\frac{4U_{dc}^2}{9((u_\alpha^*)^2+(u_\beta^*)^2)}}$	
	C_{33}		
IV	C_{41}	$\sqrt{\frac{\frac{U_{dc}^2}{3}+(\frac{u_\alpha^*}{2}-\frac{\sqrt{3}u_\beta^*}{2})^2}{(u_\alpha^*)^2+(u_\beta^*)^2}}$	$\frac{U_{dc}}{\sqrt{3(u_\alpha^*)^2+3(u_\beta^*)^2}*\cos(\arctan(\frac{u_\beta^*}{u_\alpha^*})+\pi)}$
	C_{42}	$\sqrt{\frac{4U_{dc}^2}{9((u_\alpha^*)^2+(u_\beta^*)^2)}}$	
	C_{43}		
V	C_{51}	$\sqrt{\frac{(u_\alpha^*)^2+\frac{U_{dc}^2}{3}}{(u_\alpha^*)^2+(u_\beta^*)^2}}$	$\begin{cases}\frac{U_{dc}}{\sqrt{3(u_\alpha^*)^2+3(u_\beta^*)^2}*\cos(\arctan(\frac{u_\beta^*}{u_\alpha^*})+\pi)} & u_\alpha^*\neq 0\\ \frac{U_{dc}}{\sqrt{3(u_\alpha^*)^2+3(u_\beta^*)^2}} & u_\alpha^*=0\end{cases}$
	C_{52}	$\sqrt{\frac{4U_{dc}^2}{9((u_\alpha^*)^2+(u_\beta^*)^2)}}$	
	C_{53}		
VI	C_{61}	$\sqrt{\frac{\frac{U_{dc}^2}{3}+(\frac{u_\alpha^*}{2}+\frac{\sqrt{3}u_\beta^*}{2})^2}{(u_\alpha^*)^2+(u_\beta^*)^2}}$	$\frac{U_{dc}}{\sqrt{3(u_\alpha^*)^2+3(u_\beta^*)^2}*\cos(\arctan(\frac{u_\beta^*}{u_\alpha^*})+\pi)}$
	C_{62}	$\sqrt{\frac{4U_{dc}^2}{9((u_\alpha^*)^2+(u_\beta^*)^2)}}$	
	C_{63}		

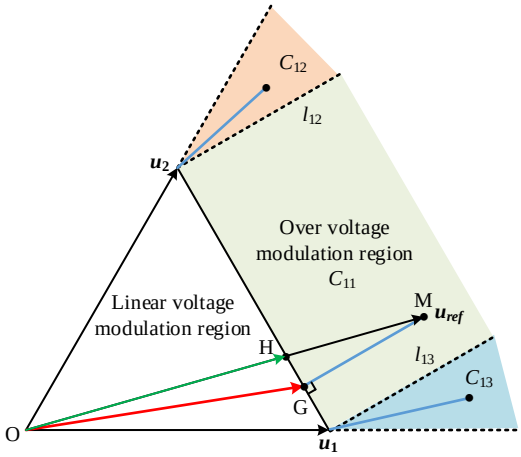

Figure 8. The diagram of OVMR.

Q3:

Compare your modulation strategies with some conventional one like SVM from the point of view of THD, harmonics, etc

Responses:

Thank you for your suggestions. We have repeated and reconstructed the whole simulation and experiment and provided the comparison tables to compare the THD, torque ripple, and CMV magnitude in Tables 7-9. Also, the experiment figures 19-26 are rearranged in format, with the proposed method shown on the left and the SVPWM shown on the right for comparison. The simulation shows that AZSPWM has the highest torque ripple and current THD, NSPWM is less than AZSPWM, and SVPWM has the smallest torque ripple with current THD. The experimental torque waveform also shows that the proposed hybrid modulation method has a larger torque ripple and current THD than the SVPWM. However, the proposed method achieves the minimum CMV peak value. Overall, through the region division and proper modulation scheme arrangement, the proposed method has the minimum CMV magnitude and also maintains the best steady-state performance.

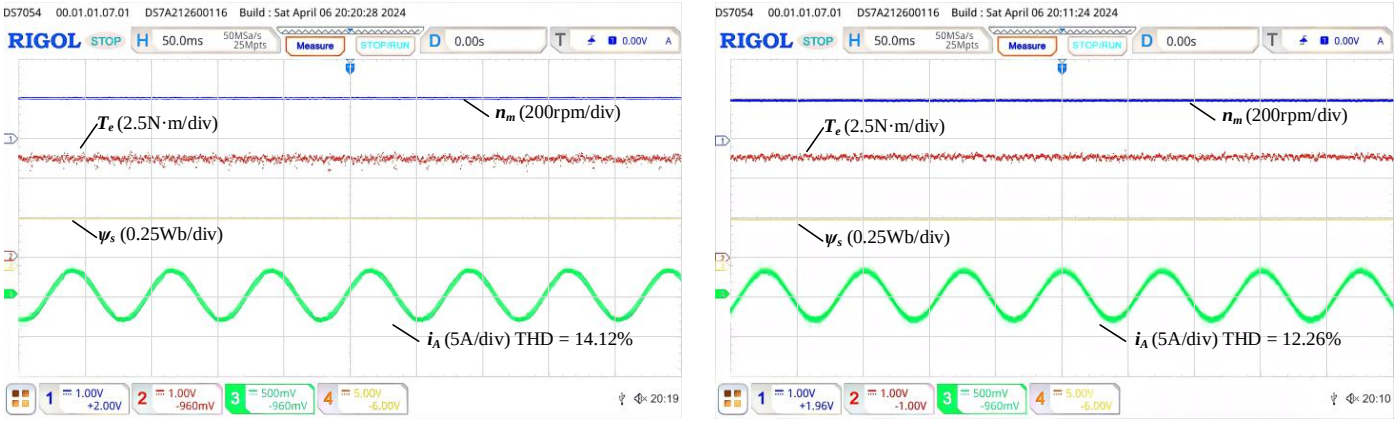

(**a**) (**b**)

Figure 19. Steady-state experimental results for the proposed method when PMSM at 200 rpm with the load of 5 N·m. (a) The proposed method. (b) SVPWM.

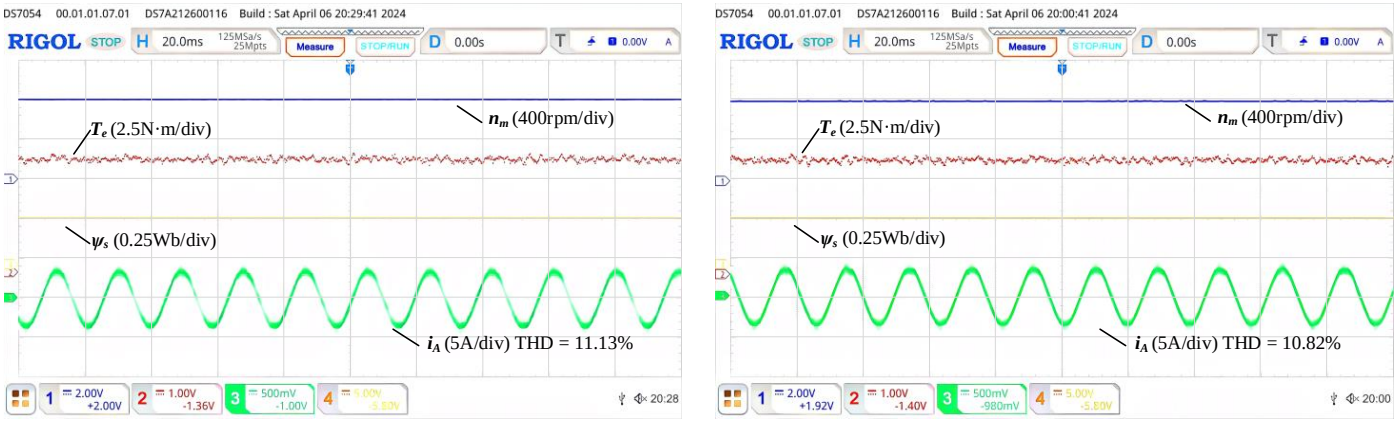

(**a**) (**b**)

Figure 21. Steady-state experimental results under AZSPWM when PMSM at 800 rpm with the load of 5 N·m. (a) The proposed method. (b) SVPWM.

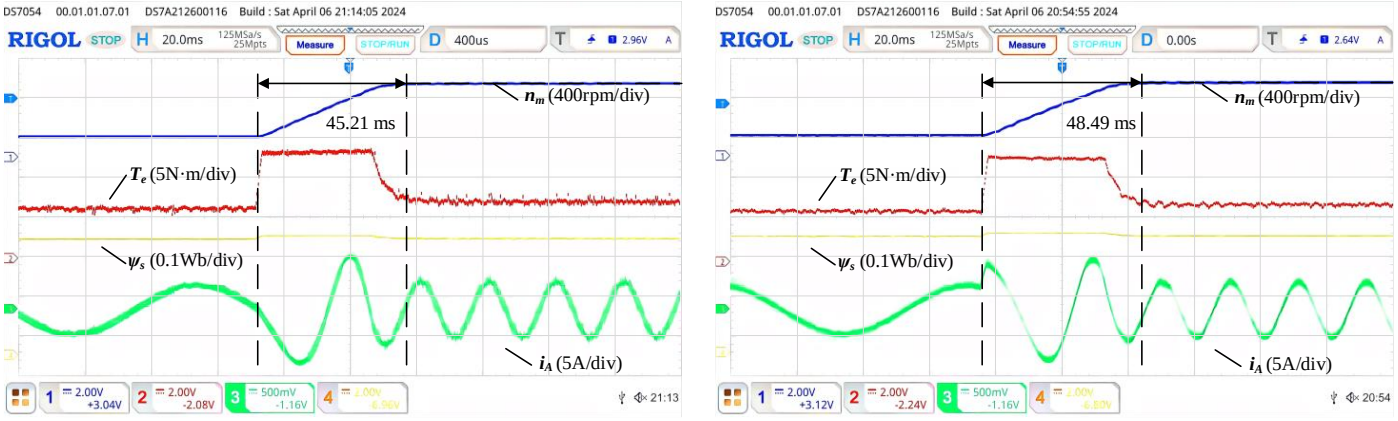

(**a**) (**b**)

Figure 23. Dynamic response experimental results with a load of 5 N·m accelerate from 200 rpm to 800 rpm. (a) The proposed method. (b) SVPWM.

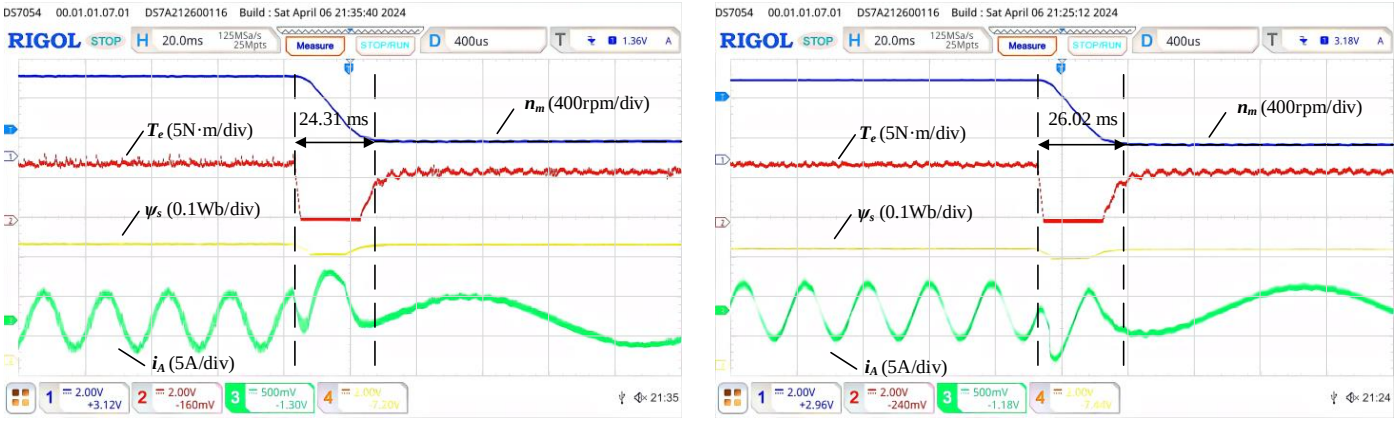

(**a**) (**b**)

Figure 24. Dynamic response experimental results with a load of 5 N·m decelerate from 800 rpm to 200 rpm. (a) The proposed method. (b) SVPWM.

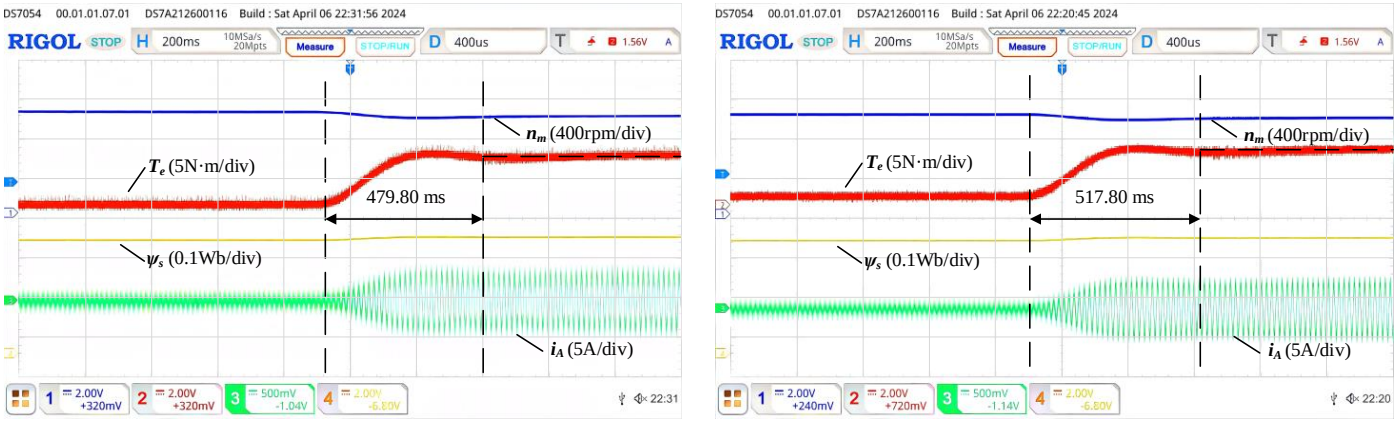

(**a**) (**b**)

Figure 25. Dynamic response experimental results at 1000 rpm increase from 0 N·m to 5 N·m. (a) The proposed method. (b) SVPWM.

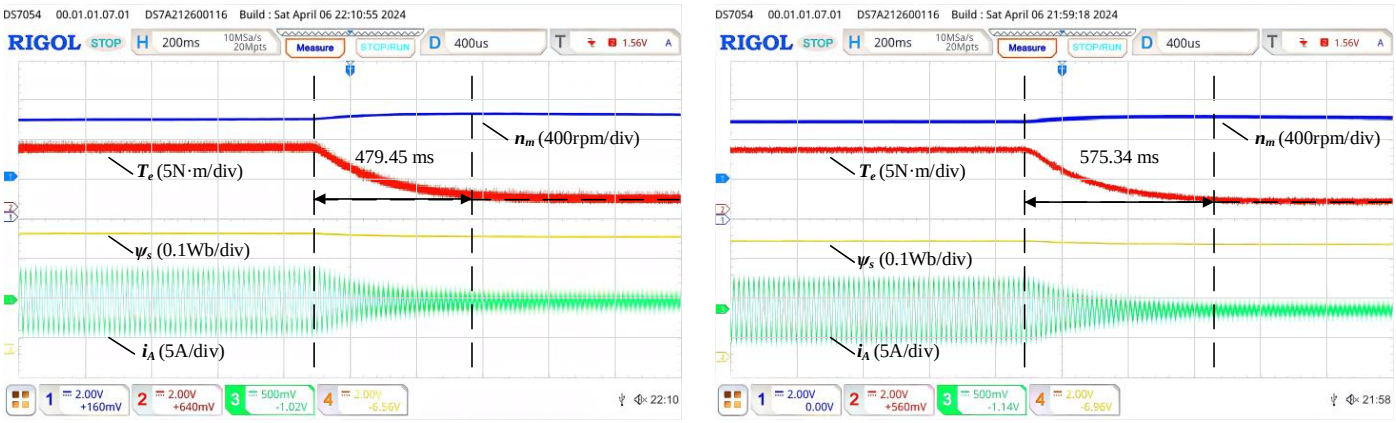

(**a**) (**b**)

Figure 26. Dynamic response experimental results at 1000 rpm decrease from 5 N·m to 0 N·m. (a) The proposed method. (b) SVPWM.

Table 7. Steady-state simulation results summary table.

Method	Operation	Current THD	Torque Ripple	CMV Magnitude
AZSPWM	200 rpm; 5 N·m	15.17 %	0.2688 N·m	46.67 V
	800 rpm; 5 N·m	13.92 %	0.2777 N·m	46.67 V
NSPWM	200 rpm; 5 N·m	13.08 %	0.1603 N·m	135.0 V
	800 rpm; 5 N·m	12.63 %	0.2283 N·m	46.67 V
SVPWM	200 rpm; 5 N·m	2.97 %	0.1076 N·m	135.0 V
	800 rpm; 5 N·m	6.05 %	0.1886 N·m	135.0 V

Table 8. Steady-state experiment results summary table.

Region	Method	Current THD	Torque Ripple	CMV Magnitude
LVMR	The proposed method	14.12%	0.0614 N·m	46.67 V
	SVPWM	12.26 %	0.0428 N·m	135.0 V
HVMR	The proposed method	11.13 %	0.0564 N·m	46.67 V
	SVPWM	10.82 %	0.0515 N·m	135.0 V

Table 9. Dynamic experiment results summary table.

Operation Condition		The proposed method	SVPWM
Speed Step	200-800 rpm	45.21 ms	48.49 ms
	800-200 rpm	24.31 ms	26.02 ms
Load Step	0-5 N·m	479.80 ms	517.80 ms
	5-0 N·m	479,45 ms	575,34 ms

Q4:

Explain better connection between dynamics of the drive and overmodulation strategy

Responses:

Thank you for your suggestion. On page 17, the part 4.3, we have discussed the connection between IOMPWM with dynamic performance in detail.

To prove the improved overvoltage modulation performance of the proposed method. The operation conditions are set to verify the effectiveness of IOMPWM, comparing with the traditional overvoltage modulation method.

First, to test the dynamic improvement of IOMPWM, set the DC-link voltage source low to 210 volts, the PMSM control speed to 1500 rpm and remain the speed PI controller and other condition the same. It focuses on the start-up process and let the reference VV locating in the OVMR. In Figure 15, the red lines represent the controlled speed reference, and the blue lines represent the PMSM speed. It shows that PMSM under IOMPWM reach and remain steadily at 1500 rpm at 0.15 seconds. However, PMSM under the conventional overvoltage modulation method cannot even reach the controlled speed. It proves that IOMPWM can better utilize the DC-link voltage and generate bigger i_q.

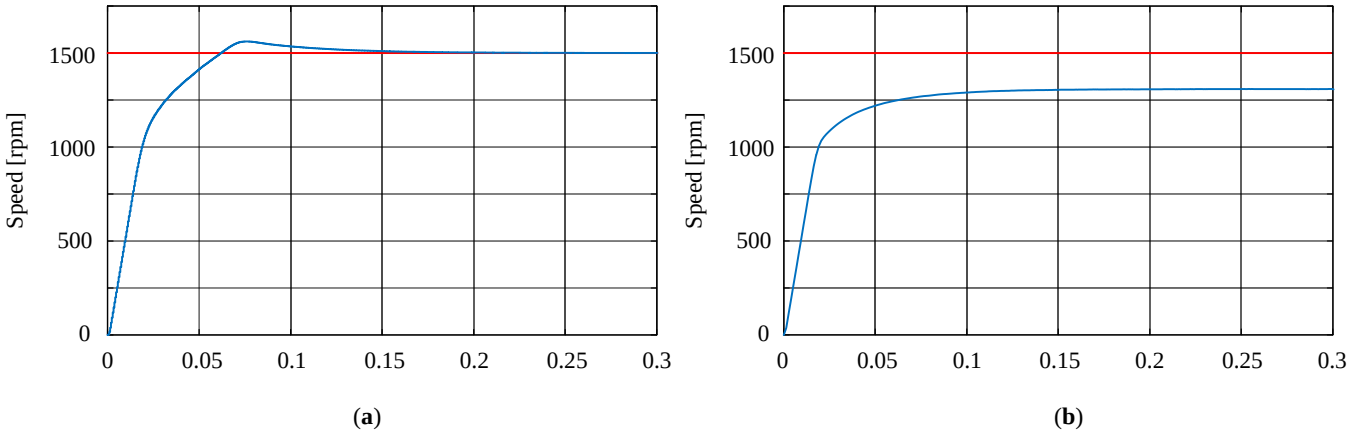

Figure 15. Harsh start-up simulation dynamic analysis at 210 V (DC-link voltage) and 1500 rpm (Control speed). (a). The proposed method. (b). Traditional overvoltage modulation method.

Second, to test the steady-state improvement of IOMPWM, set the DC-link voltage to the original value and controlled speed to 1500 rpm. It focuses on the process after the speed overshoot. In Figure 16, the red lines represent the controlled speed reference value and the blue lines represent the PMSM speed. The PMSM controlled by IOMPWM reaches and remain at the targeted speed at 0.2 s. However, the PMSM controlled by the conventional method has a bigger overshoot speed and also cannot reach the target speed even at 0.3s.

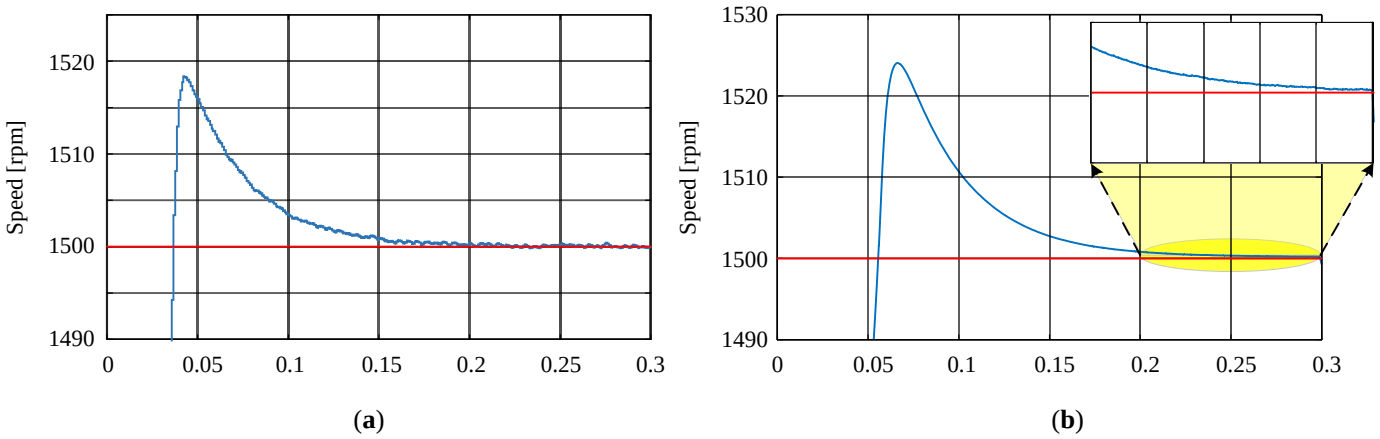

Figure 16. Start-up simulation steady-state analysis at 270 V (DC-link voltage) and 1500 rpm (Control speed). (a). The proposed method. (b). Traditional overvoltage modulation method.

Furthermore, i_q, i_q^*, $i_q(k+1)$ for traditional overvoltage modulation method are shown below. In Figure 17, i_q^* represents the reference q-axis current generate by PI speed controller, $i_q(k+1)$ represents the q-axis current generate by i_q at kT_s using IOMPWM. It shows that q-axis current i_q is always less than $i_q(k+1)$ predicted by IOMPWM. Therefore, IOMPWM has better dynamic performance than SVPWM by providing larger quadrature current.

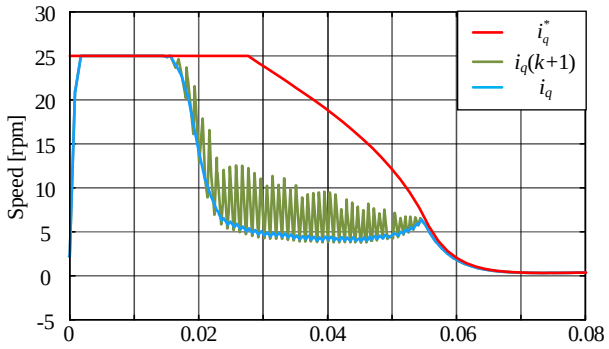

Figure 17. The diagram of OVMR.